Chemical Geology 642 (2023) 121799

Contents lists available at ScienceDirect

Chemical Geology

journal homepage: www.elsevier.com/locate/chemgeo

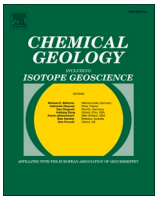

Combining methane clumped and bulk isotopes, temporal variations in molecular and isotopic composition, and hydrochemical and geological proxies to understand methane's origin in the Ronda peridotite massifs (Spain)

Lucía Ojeda [a,1], Giuseppe Etiope [b,c,1], Pablo Jiménez-Gavilán [a], Ildiko Melinda Martonos [c], Thomas Röckmann [d], Maria Elena Popa [d], Malavika Sivan [d], Antonio Fermín Castro-Gámez [a], José Benavente [e], Iñaki Vadillo [a,*]

[a] Department of Geology, Faculty of Science, University of Malaga, Malaga, Spain
[b] Istituto Nazionale di Geofisica e Vulcanologia, Sezione Roma 2, Rome, Italy
[c] Faculty of Environmental Science and Engineering, Babes-Bolyai University, Cluj-Napoca, Romania
[d] Institute for Marine and Atmospheric Research Utrecht, Utrecht University, the Netherlands
[e] Department of Geodynamics and Water Research Institute, University of Granada, Spain

ARTICLE INFO

Editor: Don Porcelli

Keywords:
Methane
Hydrogen
Hyperalkaline springs
Clumped isotopes
Ronda peridotites

ABSTRACT

In serpentinised peridotite and ultramafic rock systems, methane (CH_4) origin is frequently considered abiotic, but variable microbial and thermogenic components can also exist. Typically, the origin of CH_4 is studied using bulk, $^{13}C/^{12}C$ and $^{2}H/H$ isotopic composition, molecular gas composition, occasionally radiocarbon (^{14}C), microbiology and geological context. Recent advances in CH_4-clumped isotope methods have yielded novel insights into the formation of CH_4: nonetheless, their interpretation in natural gas samples is often uncertain and requires additional research. Here, we study the origin of the gas released in hyperalkaline (pH > 10) springs in the Ronda Peridotite Massifs (southern Spain), combining bulk and clumped CH_4 isotopes with molecular gas composition, hydrochemical (Total Organic Carbon and Platinum Group Elements in water), geothermal and geo-structural data. Five springs analysed in 2014 have been re-examined for changes in gas chemistry over time, and three newly discovered gas-bearing springs are analysed for the first time. Regardless of whether springs have microbial or abiotic isotopic fingerprints, we find that bulk CH_4 isotopes are fairly stable over a seven-year period. This suggests that the CH_4 source(s) or postgenetic processes (such as oxidation and diffusion) have not undergone significant temporal changes. Major variations in H_2 and CH_4 concentrations in certain springs may be the result of changes in gas pressure and migration intensity. Paired CH_4 clumped isotopes ($\Delta^{12}CH_2D_2$ - $\Delta^{13}CH_3D$) were analysed in two bubbling springs, where the presence of CH_4 can be interpreted as non-microbial based on ^{13}C enrichment, absence of ^{14}C, and the presence of ethane and propane. However, these isotopes are in disequilibrium, which prevents the quantification of the gas formation temperature. Within the $\Delta^{12}CH_2D_2$ - $\Delta^{13}CH_3D$ diagram, the data lie within both the microbialgenic zone, suggested by previous authors, and the abiotic zone that results combining data from laboratory gas synthesis and other natural gas samples. Therefore, attributing a microbial origin to CH_4 based only on clumped isotopes is less definite than previously assumed. The amount of Total Organic Carbon appears to be correlated with the origin of CH_4, as it is higher in ^{13}C-depleted CH_4 samples and lower in ^{13}C-enriched samples. Palladium (Pd) and Rhodium (Rh) dissolved in water (the more soluble Platinum Group Elements) can be a proxy for the chromitite ore deposits contained in plagioclase tectonite layers throughout the investigated area, which may act as catalysts for abiotic CO_2 hydrogenation. Clumped isotope disequilibrium and the reported absence of diffuse CH_4-bearing fluid inclusions in the peridotites appear to rule out high temperature gas genesis in post-magmatic inclusions. These observations, along with the moderate temperatures at the base of the peridotite massifs and the consistent occurrence of gas

* Corresponding author.
E-mail address: vadillo@uma.es (I. Vadillo).
[1] Co-First Authors.

https://doi.org/10.1016/j.chemgeo.2023.121799
Received 28 June 2023; Received in revised form 3 October 2023; Accepted 25 October 2023
Available online 28 October 2023

along tectonic contacts between serpentinised (H_2-bearing) peridotite and carbon-bearing rocks, are compatible with the theory of low-temperature CO_2 hydrogenation.

1. Introduction

The majority of natural gas used as a fuel source is biotic methane (CH_4), which is produced in sedimentary basins by microorganisms and the thermal cracking of kerogen or oil. Despite the absence of organic matter, methane is increasingly discovered in non-sedimentary habitats, such as aquifers or free gas in Precambrian shields, and surface seeps or hyperalkaline (pH > 10) springs in serpentinised ophiolites and peridotite massifs (see reviews by Etiope and Sherwood Lollar, 2013; Etiope and Whiticar, 2019; Monnin et al., 2021; Etiope and Oze, 2022). In continental environments, where serpentinization is often developed at low temperatures (<150–200 °C), three major origins have been hypothesised for the formation of CH_4: two are associated with abiotic processes, while the third is related to microbialgenesis. The first abiotic hypothesis refers to CH_4 generated at a moderate temperature (<150 °C) through Fischer-Tropsch Type (FTT) reactions, specifically CO_2 hydrogenation (or Sabatier reaction: $CO_2 + 4H_2 = CH_4 + 2H_2O$) occurring in fractures (Etiope and Oze, 2022, and references therein). Methane is produced by combining H_2 from serpentinization and CO_2 from the atmosphere, soil, carbon bearing rocks, or mantle (e.g., Etiope and Sherwood Lollar, 2013). Metal catalysts (e.g., chromium, ruthenium, iron minerals) promote the Sabatier reaction by decreasing the activation energy required for the reaction to move forward. Chromitites, which are common in ophiolites and peridotite massifs and are rich in chromium and Platinum Group Element (PGE, in particular ruthenium, a crucial catalyst for low temperature CO_2 hydrogenation; Etiope and Ionescu, 2015), contain significant amounts of H_2 (up to 22 vol% in the gas extracted by milling) and ^{13}C-enriched CH_4 ($\delta^{13}C$ from −0.5 to −20 ‰) compared to other mafic and ultramafic rocks, and have been considered as potential source rocks of abiotic gas (Etiope et al., 2018; De Melo Portella et al., 2019; Etiope and Oze, 2022). This abiotic model of CH_4 production is supported by (a) a combination of stable C and H isotope composition of CH_4 ($\delta^{13}C_{CH4}$ typically > −40 ‰, δ^2H approximately from −100 to −400 ‰; Etiope and Oze, 2022), which is distinguishable from microbial and thermogenic fingerprints; e.g., Milkov and Etiope, 2018); (b) the molecular gas composition (presence of heavier hydrocarbons and H_2); (c) the absence of radiocarbon (^{14}C) in CH_4; and (d) petrological and geological data indicating the presence of catalyst rich rocks (e.g., Cr and PGE in chromitites) and faults as preferential pathways of gas migration from depth. This model's limitations refer to the actual capacity of the metals, particularly the low-abundance PGE, to sustain considerable and persistent gas generation.

The second abiotic hypothesis refers to CH_4 synthesis at elevated temperature within fluid inclusions in olivine-rich rocks, which then migrates to the surface through seeps and springs (Klein et al., 2019; Grozeva et al., 2020). Inclusions are regarded as "reactors" in which CH_4 is produced via high-temperature (>200–300 °C) FTT synthesis following the cooling of magmatic fluids through the interaction of olivine, oxidised carbon and H_2 gas. Gas generation has been modelled using the distribution and composition of fluid inclusions in olivines (Klein et al., 2019) and the isotopic content of the gas (Grozeva et al., 2020). The shortcomings of this model include inconsistencies with the available clumped isotope analyses, which suggest temperatures of CH_4 formation lower than those taken into account in fluid inclusions (Young et al., 2017) and problems with gas flow dynamics (i.e., assuring long-lasting and continuous gas leaching from the inclusions to the surface; Etiope and Oze, 2022).

The microbial origin of CH_4 is mediated by methanogens in low-temperature aquifers utilising CO_2, formate and/or acetate (Miller et al., 2018; Nothaft et al., 2021). However, not all hyperalkaline springs contain methanogens (e.g, Tiago and Veríssimo, 2013; Suda et al., 2022), and there are currently no models explaining how microbial communities alone can produce enough fossil CH_4 and generate long-lasting high-pressure gas seeps, as those observed in a number of locations (Etiope and Oze, 2022). In this respect, the research of endoliths that may utilise ^{14}C-free substrates within deep mafic-ultramafic rocks may be useful (e.g., Fones et al., 2022), but it should include the analysis of methane, and its ^{14}C content, occluded in the rocks.

Generally, bulk isotope studies ($^{13}C/^{12}C$ and $^2H/H$ of CH_4) are used to discriminate between three major sources of CH_4: thermogenic, microbial, and abiotic. Nonetheless, overlapping isotopic signatures from different sources and difficulties in unravelling mixtures of sources or postgenetic processes have led to the association of the bulk isotopic analysis with multiply substituted "clumped" CH_4 isotopologues ($\Delta^{13}CH_3D$ and $\Delta^{12}CH_2D_2$; where D = ^{2}H, see notation in Young, 2020), which provide information on the temperature of CH_4 formation when C—H bonds are in equilibrium (e.g., Stolper et al., 2018; Young et al., 2017; Young, 2020). The relationship between $\Delta^{13}CH_3D$, $\Delta^{12}CH_2D_2$ and temperature provides a thermodynamic equilibrium reference curve in the $\Delta^{13}CH_3D$ vs. $\Delta^{12}CH_2D_2$ space (Young et al., 2017, and references therein). Data falling on the equilibrium line represent the intramolecular temperature at which CH_4 was formed or equilibrated. At temperatures >150 °C, CH_4 clumped-isotopes are more likely to be in thermodynamic equilibrium (Young et al., 2017). Departures from equilibrium may be expressed as $\Delta^{13}CH_3D$ and/or $\Delta^{12}CH_2D_2$ decrease or $^{12}CH_2D_2$ increase. Clumped isotope disequilibrium may allow the identification of kinetic isotope processes during methane generation and other post-generation processes such as mixing, clumped-isotope fractionation by molecular mass, desorption, oxidation, kinetics, tunnelling, and combinatorial effects (Röckmann et al., 2016a; Wang et al., 2016; Young et al., 2017; Taenzer et al., 2020; Young, 2020; Warr et al., 2021; Etiope and Oze, 2022).

However, the interpretation of methane clumped-isotopes is not straightforward, as a given combination of $\Delta^{13}CH_3D$ and $\Delta^{12}CH_2D_2$ values may reflect different origins and post-genetic processes (Young, 2020; Labidi et al., 2020; Warr et al., 2021). For example, it was suggested that microbial CH_4 is identifiable by a specific distribution of $\Delta^{13}CH_3D$ and low $\Delta^{12}CH_2D_2$ values (e.g., Young, 2020). On this premise, groundwater in some wells in Oman was interpreted to contain microbial methane (Nothaft et al., 2021). Nonetheless, gas in aquifers devoid of methanogens, abiotic gas produced in laboratory and thermogenic gas may exhibit clumped-isotope values within the range attributed to microbial gas (Dong et al., 2021; Zhang et al., 2021; Etiope and Oze, 2022). To better understand the overlap of biotic vs. abiotic gas in the $\Delta^{13}CH_3D$ vs. $\Delta^{12}CH_2D_2$ diagram, further clumped isotope data from natural and laboratory samples is required.

Here, we report an integrated study combining novel CH_4 clumped isotope data with other geochemical, hydrochemical and geological proxies, which may shed light on the microbial vs. abiotic conundrum. We present and discuss molecular and CH_4 isotopic (bulk and clumped) data from gas released in hyperalkaline springs of the Ronda Peridotite Massifs in southern Spain (hereafter RPM), likely the largest known exposure of subcontinental lithospheric mantle (Obata, 1980). A portion of these springs were analysed in 2014 (Etiope et al., 2016): some of them contain ^{13}C-depleted CH_4, typically associated with microbial sources; and others display ^{13}C-enriched, ^{2}H-depleted and fossil (^{14}C-free) CH_4, indicative of an abiotic origin. We have resampled the gas from five springs and studied new three gas-bearing springs discovered within the RPM in 2015 and 2021 (Fig. 1). Analyses of paired clumped isotopes of CH_4 ($^{13}CH_3D$ and $^{12}CH_2D_2$) have been performed in two bubbling springs, containing ^{13}C-enriched CH_4 (one of which is ^{14}C-free). The interpretation of methane origin is then performed by

combining the following types of information: (a) bulk and clumped isotopes of CH_4 in the context of proposed genetic zonation in the relative isotopic diagrams; (b) temporal variation of molecular and isotopic composition of the gas; (c) the relationships between springs and geo-structural and geothermal settings (e.g., presence of faults, deep temperatures); (d) the amount in the water of PGE, as potential catalysts of abiotic synthesis, and Total Organic Carbon (TOC) as potential feedstock for microbial activity.

2. Geological setting and site description

2.1. The Ronda Peridotite Massifs

The Ronda peridotites (Fig. 1) are one of the world's largest outcrops of subcontinental mantle (~450 km^2) distributed in three main massifs bounded by shear zones: Ronda ultramafic massif, Carratraca ultramafic massif and Ojen ultramafic massif. We use the term "Ronda Peridotite Massifs" or "RPM" to refer to the ensemble of the three massifs.

The Ronda peridotites are primarily composed of lherzolite with minor contributions of harzburgite, dunite, and mafic layers (Hernández- Pacheco, 1967). They crop out in the Internal Zone of the Betic Cordillera, consisting in metamorphic rocks in their westernmost part, which are grouped into the Alpujárride and the Maláguide complexes. The Alpujárride complex is composed of Los Reales unit, a metasedimentary sequence overlying the ultramafic rocks, and the Blanca unit, which includes metamorphic rocks (metapelites and marbles) underlying the peridotites (Fig. 1). The ultramafic massifs constitute a separate tectonic unit placed between Los Reales and Blanca units (Fig. 1).

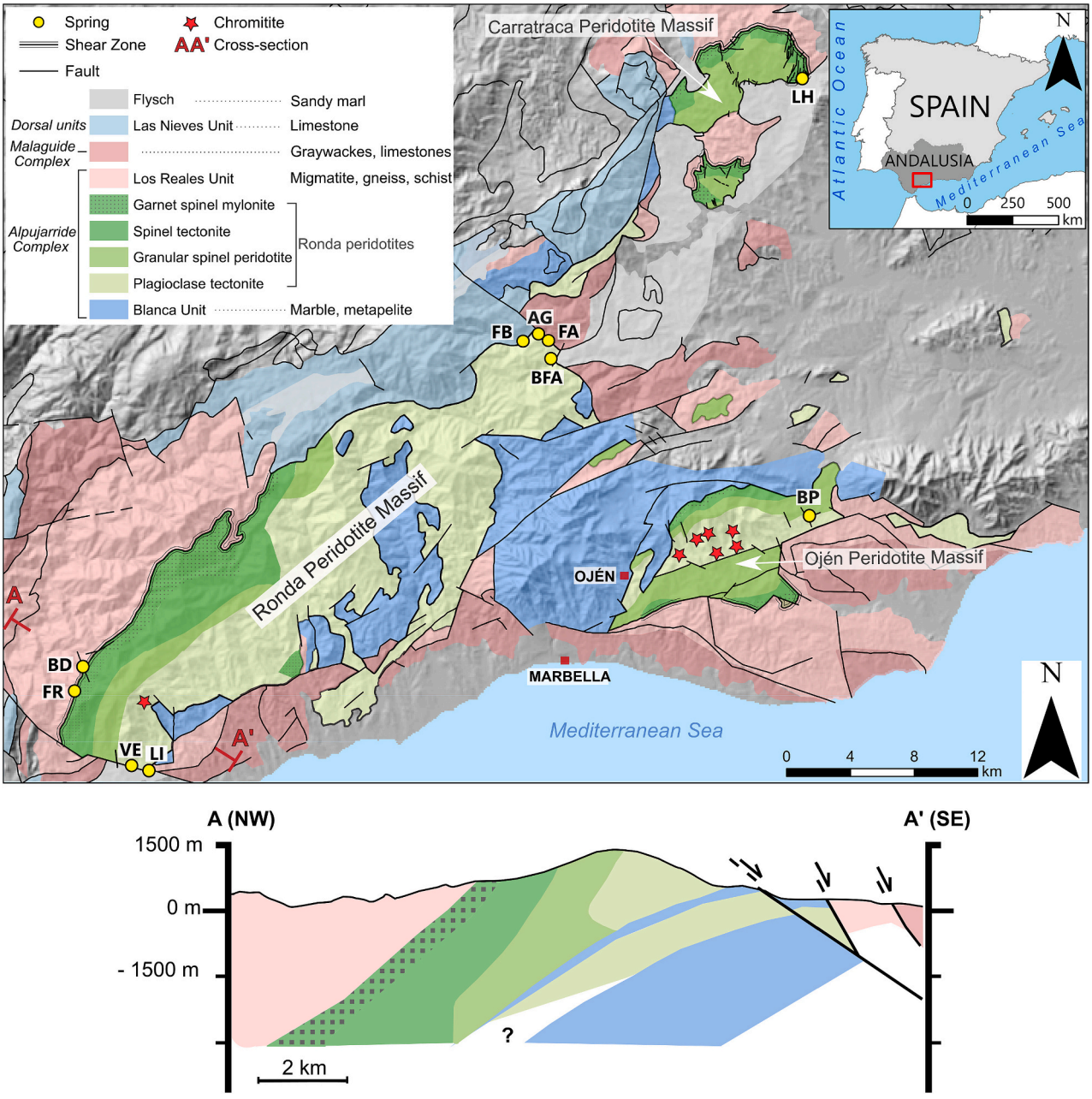

Fig. 1. Geological map showing the main tectonomorphic domains of the Ronda Peridotite Massifs (modified from Gervilla et al., 2019) and location of the investigated springs and known chromitite exposures. *Ronda Peridotite Massif*: BD: Baños del Duque; FR: Fuente Romana; VE: Vega Escondida (also known as Amargosa Mine); LI: Lucildi; FA: Fuente Amargosa; BFA: Balneario Fuente Amargosa; AG: Alfaguara; FB: Fuente de la Burbuja. *Ojen Peridotite Massif*: BP: Baños del Puerto. *Carratraca Peridotite Massif*: LH: La Hedionda. Bottom: cross-section (A-A') of the southwestern sector (redrawn from Hidas et al., 2013).

The Ronda peridotites host two types of springs: the first type, fed by shallow groundwater circulation through the weathered zone, is slightly to medium mineralised (electrical conductivity around 300–800 μS/cm), with Mg^{2+}–HCO_3^- facies, pH around 7–8, and average temperature similar to atmospheric air (Jiménez-Gavilán et al., 2021). The second type, which is investigated in this study, is less frequent and is related to the circulation of deep water along the main faults of the peridotite massifs. These springs are hyperalkaline (pH > 10), with Ca^{2+}–OH^- facies, permanent but with lower outflow (<1 L/s; Vadillo et al., 2016; Jiménez-Gavilán et al., 2021), and contain significant amounts of dissolved CH_4, in some cases with active gas bubbling (Etiope et al., 2016). Some of these springs have water residence times exceeding 2000 years (Etiope et al., 2016). Previous studies have documented that the fluids are poor in Mg^{2+} and rich in Na^+, K^+, Ca^{2+} and Cl^-; and carbonate precipitates, found in some springs, are formed by discharge and reaction with atmospheric CO_2 and/or mixing with Mg^{2+}–HCO_3^- river water (Vadillo et al., 2016; Giampouras et al., 2019). This unique hydrochemistry results in an unusual distribution of rare earth elements (REEs), restricted by the high pH and low dissolved carbon concentrations of the fluids (Zwicker et al., 2022).

2.2. The studied and newly discovered hyperalkaline springs

In this study, we investigated eight hyperalkaline springs. Five of them were reported by Etiope et al. (2016): Baños del Duque (BD), Fuente Romana (FR), Balneario Fuente Amargosa (BFA), Fuente Amargosa (FA) and Baños del Puerto (BP). Three additional hyperalkaline springs are described here for the first time: Alfaguara (AG, discovered in 2015 and analysed in 2019); Vega Escondida (VE), also known as Amargosa Mine; and Lucildi (LI, an appellation proposed combining the first names of two authors, LUCía and ILDIko). VE and LI springs were discovered in 2021 (Fig. 2). So far, we have identified 10 gas-bearing springs emerging from peridotites (Fig. 1), of which only one is not hyperalkaline (FB: Fuente de la Burbuja; Etiope et al., 2016). As a result, Andalusia appears to be the European region with the highest number of peridotite gas-bearing springs. The BD, FR, BP, AF, and LI springs emerge through rock fractures. BD, BP and LI occur along creeks, clearly connected to faults. BFA, FA and VE waters emerge from man-made pipes (BFA), fountains (FA), and horizontal tunnels (VE). All springs are located along faults (Fig. 1) and at the edge of peridotite massifs, which are in tectonic contact with metasedimentary and sedimentary (e.g., carbonates) rocks. This is studied in more detail in Section 5.3.

3. Materials and methods

In September 2021, water was collected from eight hyperalkaline (pH > 10) springs, including five springs previously examined in 2014 (Etiope et al., 2016; BD, FR, BP, FA, BFA) and three springs for which gas studies had never been conducted (AG, VE, LI). Temperature, pH, and electrical conductivity were measured in situ using a portable multiparameter probe (Hach HQ40d). Free gas from BD and BP springs (the only springs with gas bubbles) was collected using an inverted funnel connected to a three-way stopcock and syringe for injection into evacuated 120 mL glass Wheaton bottles sealed with gas-impermeable blue butyl septa (Bellco Glass Inc.) and aluminium crimp caps. At the VE spring, water was collected from the flow outside the tunnel (Fig. 2). All springs' water samples were collected and stored, without headspace, in 120 mL glass Wheaton bottles sealed with gas-impermeable blue butyl septa. The dissolved gas was then extracted by headspace method and analysed at Isotech Labs in Illinois (USA; https://isotechlabs.com/why/qaqc.html). The molecular gas composition (N_2, O_2, CO, CO_2, H_2, He, CH_4, C_2H_6 and C_3 to C_6 alkanes) was analysed by gas chromatography (Shimadzu 2010 TCD-FID, accuracy 2%). The stable carbon and hydrogen isotope composition of CH_4 ($\delta^{13}C_{CH4}$, δ^2H_{CH4}) was analysed by IRMS (Finnigan Delta Plus XL, precision ±0.1‰ for ^{13}C, ± 2‰ for ^2H).

Paired clumped isotopes of CH_4 ($\Delta^{13}CH_3D$ vs. $\Delta^{12}CH_2D_2$; delta notation as described by Young, 2020), and again bulk isotopic composition ($\delta^{13}C_{CH4}$ and δ^2H_{CH4}) were analysed in the gas from BD and BP at

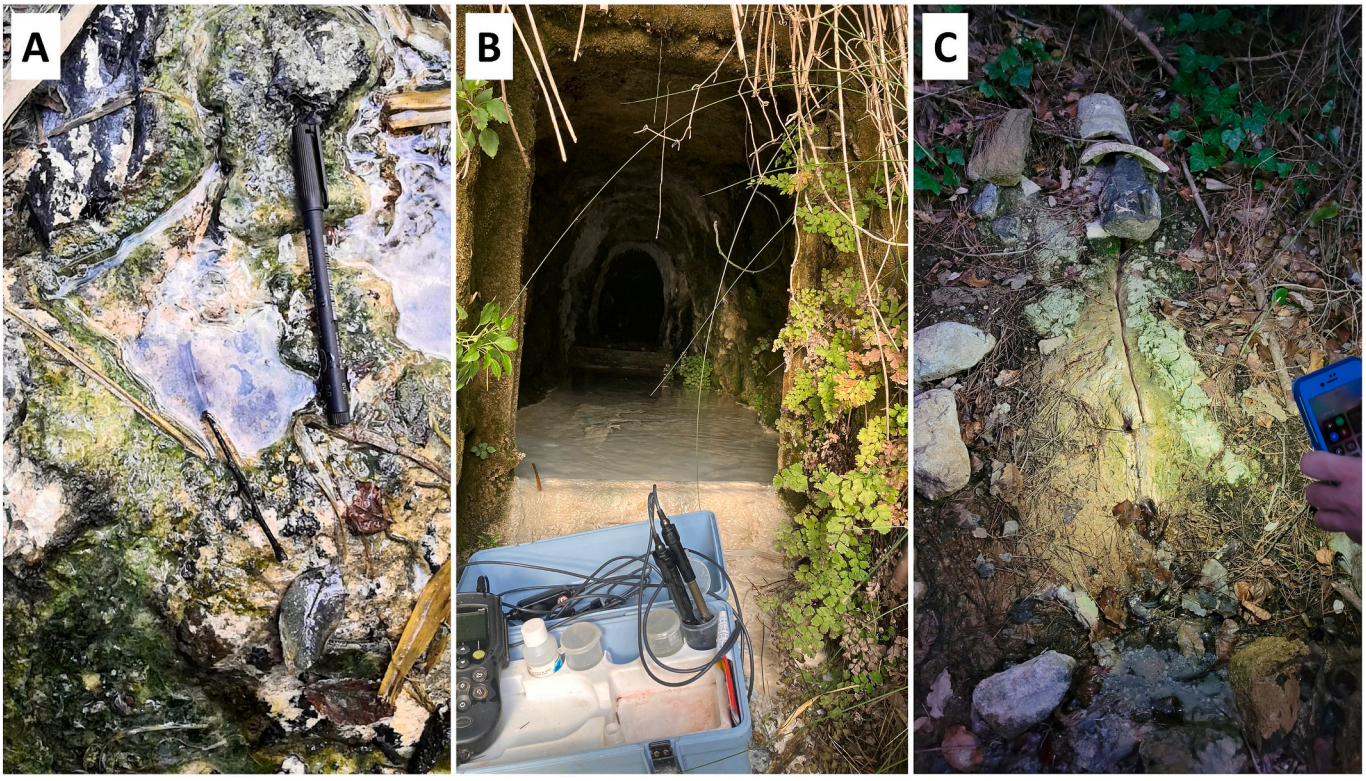

Fig. 2. The new hyperalkaline springs discovered in 2021 (A: Lucildi; B: Vega Escondida, also known as Amargosa Mine) and the spring analysed in 2019 (C: Fuente Alfaguara).

Utrecht University (the gas dissolved in the other springs was not enough for clumped isotope analysis). For bulk isotope analysis, the extracted gas samples were diluted to near-atmospheric CH_4 concentrations with synthetic air and analysed on an automated IRMS system (Brass and Röckmann, 2010; Röckmann et al., 2016b) with typical precision <0.1 ‰ for $\delta^{13}C_{CH4}$ and < 2 ‰ for $\delta^{2}H_{CH4}$ (see more details in Supplementary Material). This system has been validated in international intercomparison programmes (Umezawa et al., 2018). For clumped isotope analysis, CH_4 was separated from the bulk gas and purified, using a self-built High Concentration Extraction System (HCES) (Sivan et al., 2023). In the first step, the complete sample mixture is cryogenically collected on silica gel, and the individual components are then separated on packed gas chromatographic columns (5 m long 1/4" OD 5A molecular sieve column, separating H_2, Ar, O_2 and N_2 from hydrocarbons, and 2 m long 1/4" OD HayeSep D column, separating CH_4 from higher hydrocarbons) at 50 °C using He as the carrier gas at a flow rate of 30 mL/min, after which the purified CH_4 is collected again on silica gel. Sample amounts are chosen based on prior information on the CH_4 content (from in situ measurements and GC analyses reported in Table 1) to yield 4 mL of pure CH_4 after purification, which is presently required for a high-precision clumped isotope analysis. The clumped isotopic composition of the extracted CH_4 was analysed using a Thermo Ultra high-resolution IRMS. The typical measurement precision of a single measurement is 0.3 ‰ for $\Delta^{13}CH_3D$ and 2 ‰ for $\Delta^{12}CH_2D_2$. Multiple purifications of laboratory gas mixtures yield results within these error estimates, which indicates that the overall analytical procedure does not induce variability beyond these instrumental errors. The long-term reproducibility of the mass spectrometer is around 0.3 ‰ for $\Delta^{13}CDH_3$ and 1.7 ‰ for $\Delta^{12}CD_2H_2$. Calibration of the clumped isotope scale was performed using equilibration of laboratory CH_4 over hot catalytic surfaces at different temperatures, similar to Eldridge et al. (2019). The results are compared to the theoretical clumped isotope equilibrium values (Young et al., 2017) and agree with the experimental errors stated above. A description on temperature calibration and the reported uncertainties is provided in Supplementary Material.

Platinum Group Elements (Ir, Os, Pd, Pt, Rh, Ru) in water samples of all springs were analysed via High Resolution Inductively Coupled Plasma Mass Spectrometry (HR-ICP-MS, Element XR) on low-resolution mode (300R) in the Central Research Support Services (SCAI) at the University of Málaga. Precision achieved was on average < 4% RSD. Water samples were filtered using a 0.45 μm Millipore® filter (Merck KGaA, Darmstadt, Germany), acidified with 1 mL of 10% ultrapure HNO_3, and collected in sterile high-density polyethylene bottles (120 mL) sealed with inverted cone caps.

Total Organic Carbon (TOC), as the sum of particulate organic carbon and dissolved organic carbon (DOC), was analysed in all spring water samples by combustion (after HCl treatment) of the organic matter present in the samples using a Shimadzu V-TOC carbon analyser (precision ±0.03 mg/L). This analytical method is commonly referred to as the Non-Purgeable Organic Carbon (NPOC) method.

4. Results

4.1. Molecular gas composition

Tables 1 and 2 display the molecular composition of gas in bubbles and concentration of gas dissolved in water, respectively. In the bubbles, N_2 is abundant, while CH_4 and C_2H_6 concentrations range from 5.49 and 0.004 vol% (BD spring), to 39.86 and 0.046 vol% (BP spring), respectively. Hydrogen (H_2), propane (C_3H_8) and butane (C_4H_{10}), together with He, CO_2, and CO (not included in table) are below detection limits (see Table 1 caption). Dissolved CH_4 concentrations range from 0.54 mg/L to 3.20 mg/L, with the lowest concentration measured at LI spring and the highest concentration at FR spring. C_2H_6 concentration ranges from 0.0003 mg/L (BD, FR) to 0.039 mg/L (VE), while C_3H_8 has concentrations between <0.0005 mg/L (FR) and 0.0086 mg/L (VE). Basically, VE and LI springs (those discovered in 2021) have the highest hydrocarbon concentration, and FR has the lowest hydrocarbon concentration. H_2 was detected only in BFA, AG and VE. CO_2 and CO are below detection limits in all springs, confirming the previous analyses in Etiope et al. (2016).

Table 1
Molecular composition of gas bubbles in Baños del Duque (BD) and Baños del Puerto (BP) springs. H_2, He, CO_2, CO and C3+ hydrocarbons are below detection limits (<10, 10, 50, 100 and 5 ppmv, respectively).

Spring	Sample type	N_2	CH_4	C_2H_6
		Vol%	Vol%	Vol%
BD bubble	Gas	94.50	5.49	0.0040
BP bubble	Gas	60.09	39.86	0.0460

Table 2
Concentration of hydrogen, methane, ethane and propane dissolved in water springs. BD: Baños del Duque; FR: Fuente Romana; BP: Baños del Puerto; FA: Fuente Amargosa; BFA: Balneario Fuente Amargosa; AG: Alfaguara; VE: Vega Escondida; LI: Lucildi. Data of La Hedionda and Fuente de la Burbuja springs, not analysed in 2021, are in Etiope et al. (2016). He, CO_2, CO and C4+ hydrocarbons are below detection limits (< 10, 50, 100 and 5 ppmv, respectively, in the extracted gas phase).

Spring	Sample type	H_2	CH_4	C_2H_6	C_3H_8
		mg/L	mg/L	mg/L	mg/L
BD	Water	bdl	0.75	0.0003	0.00091
FR	Water	bdl	0.54	0.0003	< 0.0005
BP	Water	bdl	1.80	0.0046	0.0025
FA	Water	bdl	1.20	0.0059	0.0046
BFA	Water	0.01	1.70	0.0016	0.0023
AG	Water	0.05	1.20	0.0026	0.0027
VE	Water	0.01	2.50	0.0390	0.0086
LI	Water	bdl	3.20	0.0026	0.0005

Table 3
Stable C and H isotopic ratios of methane in the RPM springs. Abbreviations as in Fig. 1. Data of 2014 are from Etiope et al. (2016). The last column indicates the laboratory that carried out the isotopic analyses (UVIC: University of Victoria; ISOT: Isotech Labs; ILUU: Isolab Utrecht University).

Site	$\delta^{13}C$-CH_4	$\delta^{2}H$-CH_4	Laboratory
BD water 2014	−13.9	−333.4	UVIC
BD water 2021	−15.0	−320.0	ISOT
BD bubble 2014	−14.7	−333.0	UVIC
BD bubble 2021	−14.4	−302.0	ISOT
BD bubble 2021	−14.4	−336.2	ILUU
FR water 2014	−12.3	−287.0	UVIC
FR water 2021	−15.4	−292.0	ISOT
BP water 2014	−28.8	−309.0	UVIC
BP water 2021	−29.2	−296.0	ISOT
BP bubble 2014	−29.9	−299.7	ISOT
BP bubble 2014	−29.5	−309.0	UVIC
BP bubble 2021	−28.9	−294.0	ISOT
BP bubble 2021	−28.9	307.8	ILUU
FA water 2014 March	−68.5	−312.0	UVIC
FA water 2014 June	−69.7	−301.0	UVIC
FA water 2021	−69.6	−295.0	ISOT
BFA water 2014 March	−56.5	−316.0	UVIC
BFA water 2014 June	−59.3	−319.0	UVIC
BFA water 2021	−54.5	−318.0	ISOT
LH water 2014 March	−45.3	−192.0	UVIC
LH water 2014 June	−43.9	−180.0	UVIC
FB bubble 2014	−37.0	−280.0	UVIC
AG water 2019	−61.0	−319.7	ISOT
AG water 2021	−62.6	−319.0	ISOT
VE water 2021	−12.5	−290.0	ISOT
LI water 2021	−12.7	−292.0	ISOT

4.2. Stable C and H isotope composition of CH_4

The bulk isotopic compositions of CH_4 are provided in Table 3 and Fig. 3, which include a comparison with the data of 2014 from springs BD, FR, BP, FA, BFA, LH, and FB (Etiope et al., 2016). Fig. 3 shows that the CH_4 isotopic composition has not changed significantly after 7 years, from 2014 to 2021. FA, AG, and BFA constitute a group that looks to be dominated by microbial gas, whereas FB, BP, FR, BD, VE, and LI belong to the more typical genetic zonation of abiotic gas (Etiope and Sherwood Lollar, 2013; Milkov and Etiope, 2018; Etiope and Whiticar, 2019). The spring LH (examined only in 2014) contains ^{2}H-enriched CH_4, which is more typical of thermogenic gas.

4.3. Paired clumped isotopes of CH_4

The results for clumped isotopes are reported in Table 4 and Fig. 4. BP and BD have similar $\Delta^{12}CH_2D_2$ values (−19.9 and − 20.3 ‰), while BD has a slightly higher $\Delta^{13}CH_3D$ value (2.97 vs. 2.01 ‰). Both samples lie below the thermodynamic equilibrium line in the $\Delta^{13}CH_3D$ vs. $\Delta^{12}CH_2D_2$ space, and within the microbial (Young, 2020) and abiotic (Etiope and Oze, 2022; Zhang et al., 2021) fields obtained from laboratory studies and natural habitats.

4.4. Hydrochemistry, TOC and PGE

The springs have pH values between 10.89 and 11.72. Temperatures range from 18.5 to 22.5 °C, and electrical conductivity from 431 to 1399 µS/cm (Table 5). These data are similar to those analysed in 2014 (pH: 10.54–11.74; T: 16.8–21.5 °C; EC: 450–1366 µS/cm; Etiope et al., 2016). The TOC concentrations vary from 0.1 to 6.3 mg/L (Table 5). Among the PGE, only Rh and Pd have been detected in water, with concentrations from 2.6 ng/L to 22.7 ng/L, and from 28.9 ng/L to 250.1 ng/L, respectively (Table 5).

Table 4
Paired clumped isotopes of CH_4 from Baños del Duque (BD) and Baños del Puerto (BP) in the RPM.

Spring	$\Delta^{13}CH_3D$ (‰)	Error	$\Delta^{12}CH_2D_2$ (‰)	Error
BD bubble 2021	2.97	0.4	−19.9	2.0
BP bubble 2021	2.01	1.6	−20.3	5.4

5. Discussion

5.1. Molecular and CH_4 isotopic composition and their temporal variability

For the springs BD, FR, BP, FA, and BFA, it has been possible to assess the differences in the molecular gas composition and CH_4 isotopic signature compared to 2014 studies (Etiope et al., 2016). Dissolved gas concentrations in these spring waters are generally within the same order of magnitude as those measured in 2014. Variations in sampling, differences in analytical instrumentation, and air contaminations (for example, compositional data in Etiope et al., 2016 include O_2, meaning they were not corrected for air contamination during sampling) might have accounted for some differences between the 2014 and 2021 studies that merit consideration. While the hydrocarbons have, more or less, the same concentrations, and CO_2 is always below detection limit, H_2 was detected in the FA spring in 2014 (1.2 mg/L) (Etiope et al., 2016) but not in 2021 (Table 2). In BFA, H_2 was up to 0.16 mg/L in 2014 (Etiope et al., 2016), and 0.01 mg/L in 2021.

In the gas bubbles, the amount of CH_4 concentration in BD was 3.7 vol% in 2014 (not corrected for air contamination, as O_2 was not measured) and 5.5 vol% in 2021 (after air correction); for BP, CH_4 was up to 8.7 vol% in 2014 (or 12.4 vol% after air correction as the N_2/O_2 ratio was available; see Table 2 in Etiope et al., 2016) and 39.9 vol% in 2021. The difference of H_2 in FA and BFA, and of CH_4 in BP, over a

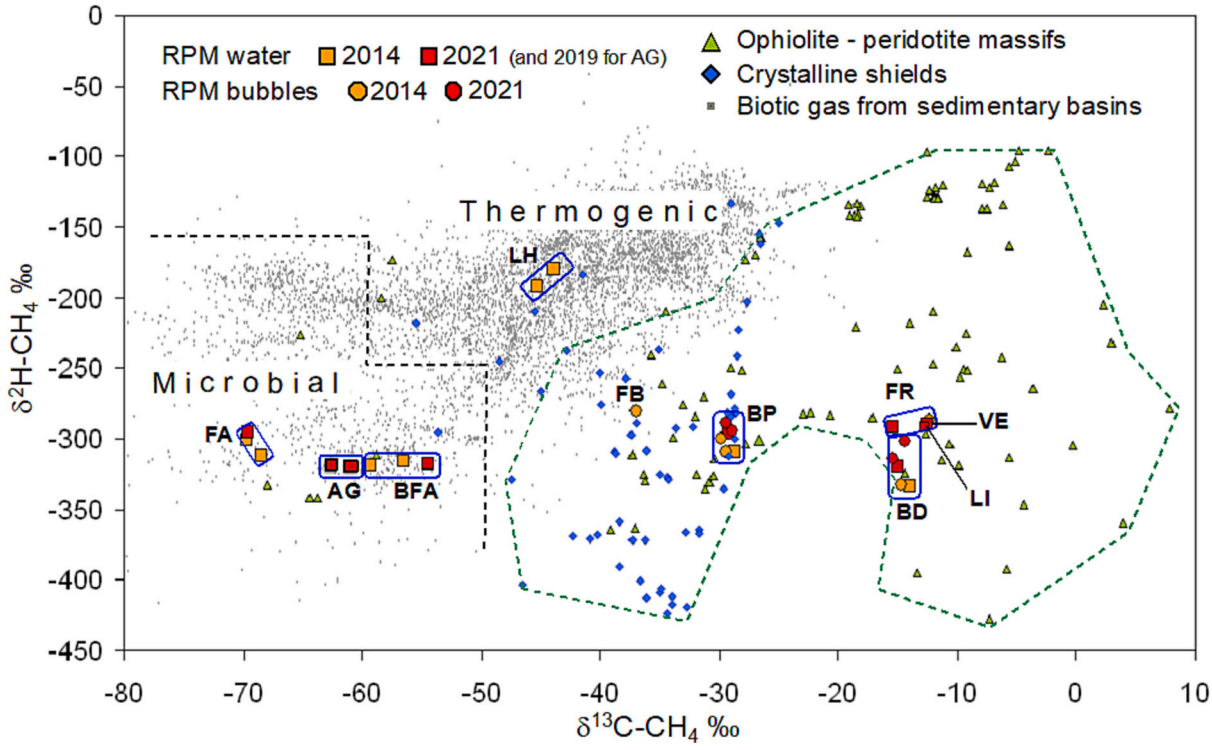

Fig. 3. Stable carbon and hydrogen isotope ratios of methane in the RPM springs (abbreviations as in Fig. 1), compared with other gas-bearing sites in continental ultramafic rock systems: ophiolites and peridotite massifs (green triangles, data from Etiope and Oze, 2022), Precambrian shield data considered dominantly abiotic (blue diamonds, from Sherwood Lollar et al., 2006), and natural gas in sedimentary basins (grey dots, global dataset from Milkov and Etiope, 2018). (For interpretation of the references to colour in this figure legend, the reader is referred to the web version of this article.)

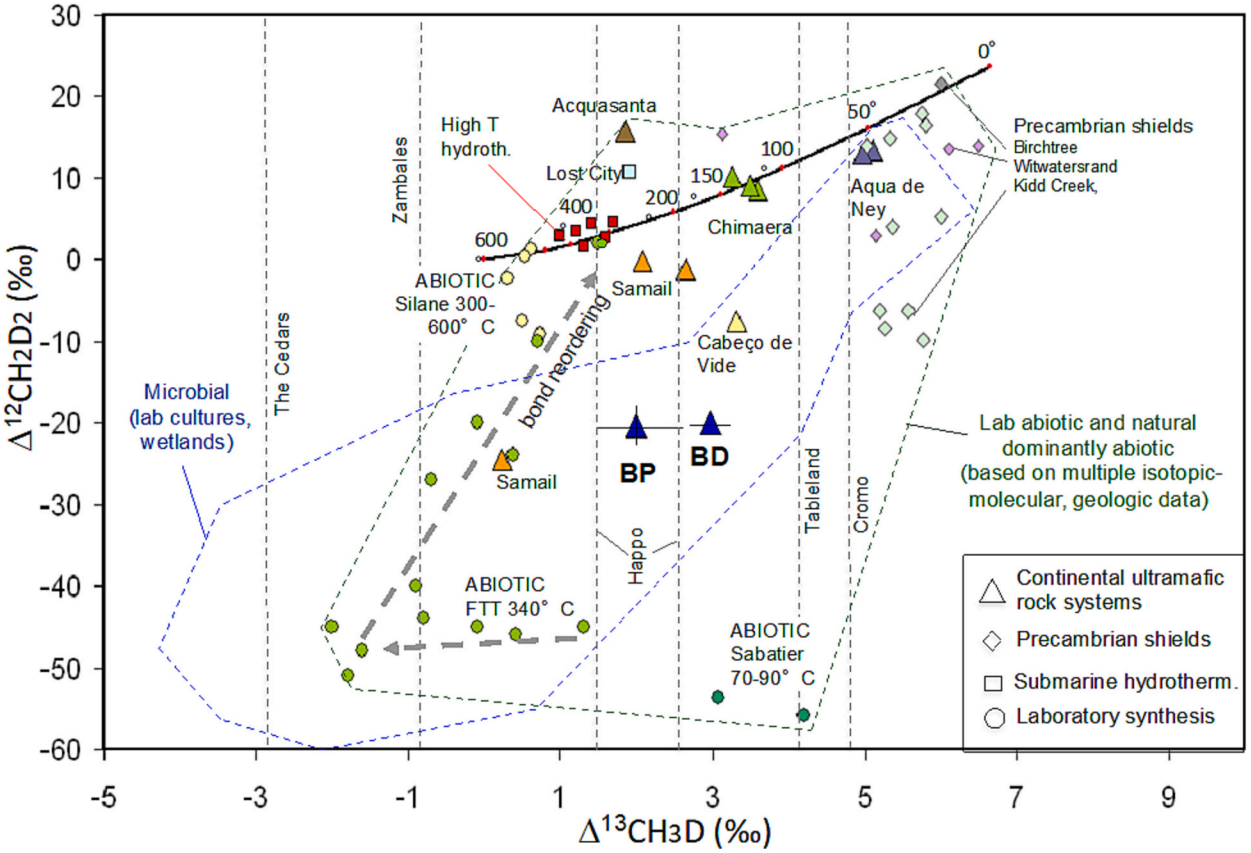

Fig. 4. $\Delta^{13}CH_3D$ vs $\Delta^{12}CH_2D_2$ data of Baños del Duque (BD) and Baños del Puerto (BP) in the framework of known CH_4 clumped-isotope distribution in gas from continental ultramafic rock systems, Precambrian shields, submarine hydrothermal fields, abiotic gas laboratory experiments and microbialgenesis (modified from Etiope and Oze, 2022). Vertical grey dashed lines are continental ultramafic systems where only $\Delta^{13}CH_3D$ was measured (all references in Etiope and Oze, 2022).

Table 5
Temperature, pH, electrical conductivity (EC), total organic carbon (TOC) and Platinum-Group-Elements (Pd and Rh) in water springs. Abbreviations as in Fig. 1. Ru, Au, Ir, Os and Pt, not shown, are below detection limit (3.7 ng/L, 0.5 μg/L, 8.3 ng/L, 59.4 μg/L, 3.9 ng/L, respectively).

Spring	Sample type	T	pH	EC	TOC	Pd	Rh
		° C		μS/cm	mg/L	ng/L	ng/L
BD	Water	18.5	11.3	513	0.3	88.4	7.5
FR	Water	19.3	11.4	526	0.1	74.7	6.0
BP	Water	21.8	11.3	671	0.1	71.8	7.2
FA	Water	21.4	11.7	1269	2.6	250.1	22.7
BFA	Water	21.8	10.9	431	6.2	28.9	2.6
AG	Water	22.5	11.7	1152	6.3	178.1	15.0
VE	Water	21.3	11.6	1399	0.4	71.7	5.7
LI	Water	22.0	11.5	958	0.1	103.1	8.4

period of seven years, may indicate variability of the gas pressure, i.e., changes in gas migration intensity and pulsations, which are typical of natural gas seepage (e.g., Wyatt et al., 1995; Etiope and Oehler, 2019; Etiope, 2023) and/or of microbial consumption. The presence of a certain gas at the surface (for example H_2, which is more sensitive to interactions with the aquifer) may be observed at specific times but not at others. It is worth noting that the H_2 concentration detected in 2014 in FA (1.2 mg/L, corresponding to about 2700 ppmv in the headspace extracted from water and analysed by the SEOS laboratory of Biogeochemistry Facility of University of Victoria; Etiope et al., 2016) is a relevant amount and comparable to H_2 observed in the Tablelands (Canada; 0.5–1.2 mg/L) and Happo (Japan; 0.3–1.3 mg/L) springs (Szponar et al., 2013; Suda et al., 2014). Although FB is only 1.8 km away from FA (see Fig. 1), its gas does not contain measurable amounts of H_2. As a result, H_2 concentrations seem to be site-specific and may vary significantly locally and over time within the same peridotite massif. This implies that, in order to have a better knowledge of the gaseous potential of a given site, the gas analysis should be repeated over time, if possible at multiple points of fluid discharge, either in water or in the presence of bubbles.

Concerning the CH_4 bulk isotopic composition, Fig. 3 shows no relevant changes in the springs analysed in 2014 and 2021. This may indicate that there are no substantial changes in the CH_4 source/s or in the effect of post-genetic processes, such as oxidation, diffusion, and mixing, which may alter the stable C and H isotope composition. However, zooming on BP and BD springs (see Supplementary Fig. S1) reveals that, while $\delta^{13}C$-CH_4 is relatively stable over time, $\delta^{2}H$-CH_4 increased up to 35 ‰ either in gas bubbles or water. This could be a result of the variable re-equilibration of hydrogen of CH_4 with water, depending on the residence time of the gas in the aquifer and gas pressure, which is consistent with the previously described variability of gas migration. Microbial activity may also alter isotopic H_2 composition. The fact that CH_4 isotopes did not significantly change over time is compatible with the relatively intense and continuous migration of gas, which is clearly advective (i.e., driven by pressure gradients). While diffusion (driven by concentration gradients) induces isotopic fractionation of gas, advection (especially in terms of bubble flows) does not modify the gas isotopic composition (e.g., Etiope et al., 2009). In fact, all the studied springs are associated with faults, which provide pathways for the upward advection of water and gas to the surface. Etiope et al. (2016) reported flux measurements of gas seepage near the BP spring associated with secondary faults, permeable to gas transport.

5.2. Unravelling gas origin within CH_4 isotopic diagrams

Paired clumped isotopes of CH_4 ($\Delta^{13}CH_3D$ vs. $\Delta^{12}CH_2D_2$) have been analysed in two ^{13}C-enriched gas samples (BP and BD) to provide insight into the temperature of CH_4 formation, and to verify whether they are compatible with the origin suggested by the bulk isotope diagram. However, methane in both BP and BD exhibits clumped-isotope disequilibrium (Fig. 4) and it is not possible to assess its formation temperature. Similar cases of disequilibrium were observed in several CH_4-bearing springs or seeps in ultramafic rocks, such as Cabeço de Vide (Portugal), Samail (Oman) and Acquasanta (Italy) hyperalkaline springs (Fig. 4; all references in Etiope and Oze, 2022). Formation temperature was determined for CH_4 of Chimaera seep (130 °C; Young et al., 2017) and Aqua de Ney spring (50 °C; Blank et al., 2017), both predominantly considered abiotic. Both BP and BD samples exhibit depletions in $\Delta^{12}CH_2D_2$ of about 30‰ relative to equilibrium (assuming formation temperatures within 100–150 °C; Table 4; Fig. 4), similar to those observed in some samples at Kidd Creek, Canada (interpreted as dominantly abiotic; Young et al., 2017) and Samail ophiolite, Oman (Nothaft et al., 2021). The Samail samples have been interpreted as microbial in origin, based on the microbialgenic zonation in the $\Delta^{13}CH_3D$ vs. $\Delta^{12}CH_2D_2$ diagram (the dashed blue line in Fig. 4), proposed by Young (2020). Nonetheless, this zonation mostly overlaps with a region containing thermogenic gas from pyrolysis (Dong et al., 2021) and abiotic gas such as that created in the laboratory by Fischer-Tropsch-Type reactions (Zhang et al., 2021; see also Etiope and Oze, 2022 for a wider discussion). Young et al. (2017) observed, at low temperatures (70–90 °C), substantial deficits in $^{12}CH_2D_2$ relative to equilibrium (theorised to be the result of "tunnelling") in gas samples produced by the Sabatier reaction with ruthenium (the same samples generated and discussed in Etiope and Ionescu, 2015). The proposed "microbialgenic zone" also contains samples where no methanogens have been found, such as Cabeço de Vide (Portugal), whose bulk isotopic and hydrocarbon compositions suggest an abiotic origin (Tiago and Veríssimo, 2013; Etiope et al., 2013). The $\Delta^{13}CH_3D$ value of BP is also within the range of the Happo springs (Japan; see Fig. 4), where methanogens are absent and the origin has been considered dominantly abiotic (Suda et al., 2022). Notable is that BP CH_4 is ^{14}C-free, i.e., fossil (Etiope et al., 2016), similar to Chimaera, Lost City, Zambales, Acquasanta and Happo (see references in Etiope and Oze, 2022). Since the circulating waters (where methanogens can operate) contain measurable levels of ^{14}C (Etiope and Oze, 2022), fossil CH_4 cannot have originated in those waters (and thus not from the microbes therein). The clumped-isotope disequilibrium, which is frequent in CH_4 generated at low temperature (Young et al., 2017), is compatible with the low geothermal gradient of the RPM region (max 23 °C/km; Fernàndez et al., 1998), suggesting extrapolated temperatures below 120 °C at the base of the 4.5 km deep peridotite body (García-Dueñas et al., 1992). Although thermogenic gas, as mentioned earlier, may display CH_4 clumped isotope values similar to BP and BD (Dong et al., 2021), a thermogenic origin for BP and BD gas is poorly plausible based on their CH_4 bulk isotopic composition, which deviates from the typical signatures of catagenetic processes (Fig. 3). It is unlikely that any ^{13}C-enriched and ^{2}H-depleted methane from ultramafic rocks can be attributed to a thermogenic source, particularly considering that the data falls outside the established thermogenic zone in the $\delta^{13}C$ vs. $\delta^{2}H$ diagram (Fig. 3). Furthermore, the presence of ethane and propane rules out a predominant microbial origin, as the production of these alkanes by microbes is rare and only occurs under specific conditions in seafloor sediments (Oremland et al., 1988; Hinrichs et al., 2006; Xie et al., 2013). It is important to note that ethanogens and propanogens have never been reported in hyperalkaline waters.

In conclusion, the isotopic and compositional data converge to suggest that the gas released by BD and BP (which is also ^{14}C-free; Etiope et al., 2016) is likely abiotic in origin, as initially proposed in Etiope et al. (2016).

5.3. The relationships between gas-bearing springs, faults and surrounding rocks

The gas-bearing hyperalkaline springs appear systematically associated with faults or shear zones (Fig. 1) where peridotites are in contact with metasedimentary or carbonate rocks.

The springs BD, FR, VE, LI, with isotopic signatures typical of abiotic CH_4, are located southwest of Sierra Bermeja, and are associated with faults near the contact of the shear zone (BD and FR) and normal low angle faults (LI and VE; Fig. 1), all related to an extensional event during orogenic accretion (Platt et al., 2013). The shear zone brought the peridotites into contact with a sequence that is a part of the continental crust (Los Reales unit), specifically with mylonitic gneisses. In some cases, the shear zone delineates the contact between peridotites and flysch (sandy marl materials), as in LH spring (Fig. 1), although the flysch complex is also found overlain by the peridotites through normal low-angle faults, as in VE and LI. The LI spring emerges from fractures along a creek (Arroyo de Polvitos) controlled by a secondary fault and located in a sector where Los Reales unit and the flysch complex converges through a set of normal low-angle faults (Fig. 1).

The springs AG, FA, BFA and FB, where CH_4 appears to be predominantly of biotic origin, occur in the northeast sector of the Ronda Ultramafic Massif, next to rivers (AG, FA, FB in Río de los Horcajos; BFA in Arroyo de los Caballos, Fig. 1) that coincide with faults. In these springs, the contact of the peridotites is with carbonate materials, mostly massive dolomites (as in FB; Las Nieves unit; Fig. 1) and graywackes with intercalated limestone levels (AG, FA; Maláguide unit; Fig. 1). In all cases, the springs occur along faults, generally at the boundaries of peridotite massifs. These locations would be optimal for the mixing and reaction of H_2 (from serpentinization of peridotite) and CO_2 (from external sedimentary rocks), as predicted by abiotic CO_2 hydrogenation models (Etiope and Oze, 2022, and references therein).

5.4. Additional proxies for gas origin and uncertainties

With reference to the three potential origins of methane discussed in Introduction (abiotic from low temperature catalysed CO_2 hydrogenation, abiotic from magmatic cooling in fluid inclusions, and microbialgenesis in the aquifer), here, we examine the interpretative role of TOC and PGE in water, and preliminary information on the availability of methanogens in the water and fluid inclusion in the RPM.

5.4.1. Potential microbialgenesis

FA, AG, and BFA exhibit CH_4 isotopic compositions consistent with the presence of microbial gas. Preliminary microbiological data, based on total DNA sequencing, are available for AG spring (Costa, 2018), which confirmed the presence of methanogens. In particular, *Methanobacterium* sp., a hydrogenotrophic methanogen that can utilise hydrogen and carbon sources, such as formate, to produce methane (Woycheese et al., 2015; Brazelton et al., 2017), was detected. This is compatible with the microbial signature of the CH_4 isotopic composition (Fig. 3). However, the presence of ethane and propane in all springs (Tables 1 and 2) suggests, as mentioned earlier, that the gas is not entirely microbial. AG hosts methanotrophs (Costa, 2018), whose presence may, in theory, contribute to increase the $\delta^{13}C$ values of the residual methane as a consequence of microbial oxidation (Miller et al., 2016). However, AG does not show an appreciable ^{13}C-enrichment (Fig. 3), which may suggest that the processes operate in an open system. We cannot dismiss the possibility that the ^{13}C-enriched CH_4 samples may contain minor amounts of microbial gas. The question of whether ^{13}C-enriched CH_4 can be entirely microbial (which could theoretically occur only in closed systems) remains a subject of debate (see Miller et al., 2016; Etiope, 2017; Miller et al., 2018). Numerous ^{13}C-enriched gas serpentinization sites exhibit the presence of alkanes heavier than methane, which contradicts the notion of the gas being solely of microbial origin (Etiope, 2017; Etiope and Whiticar, 2019). Nevertheless,

microbiological analyses should be conducted in the other RPM springs to help in the interpretation of the bulk isotope data.

5.4.2. The role of TOC and its possible implication in the origin of the gas

Notably, TOC concentrations in the waters with microbial CH_4 (FA, BFA and AG, ranging from 2.6 to 6.3 mg/L; Table 5 and Fig. 5) are higher than in the springs with predominantly abiotic gas (BD, FR, BP, VE, LI, ranging from 0.1 to 0.4 mg/L). TOC data are poorly available in the literature for other hyperalkaline springs, where DOC or DIC are more often analysed. TOC was reported from Oman and Liguria ophiolite springs with a median concentration of 1.3 mg/L for 11 locations (Chavagnac et al., 2013), where gas is generally abiotic (Etiope and Oze, 2022 and references therein). It is known that TOC increases in rocks with sedimentary components, often exceeding 5–10 mg/L (Gooddy and Hinsby, 2008). Anyway, also DOC, which is a fraction of TOC, is generally lower in ^{13}C-enriched CH_4 bearing springs (e.g., 0.1 to 0.8 mg/L in Zambales; Cardace et al., 2015), compared to hyperalkaline springs with biotic (microbial or thermogenic) CH_4 (e.g., 0.24 to 2 mg/L, as in The Cedars, California; Morrill et al., 2013; and Tablelands; Szponar et al., 2013). Although specific organic fractions contributing to TOC have not been measured in the RPM samples, it is known that organic acids such as formate and acetate, which can be major components of DOC in gas-bearing fluids (McDermott et al., 2015; Sherwood Lollar et al., 2021) are the substratum for methanogenesis. Methanogens belonging to family *Methanobacteriaceae* and *Methanosarcinales*, the most abundant methanogenic microorganisms detected in hyperalkaline waters, seem to use preferentially formate as substrate for methanogenesis (Brazelton et al., 2017). Therefore, elevated TOC appears to be a potential proxy of CH_4 microbialgenesis. In contrast, low TOC values in hyperalkaline waters with ^{13}C-enriched and ^{14}C-free CH_4 would be compatible with an abiotic gas origin.

5.4.3. Dissolved PGE as a proxy of catalyst availability for abiotic methane synthesis

Abiotic CH_4 formed at low temperatures via catalysed CO_2 hydrogenation is favoured by metal catalysts such as Cr, Ru and Rh, primarily found in chromitites (Etiope et al., 2018; De Melo Portella et al., 2019). In the RPM, Ru and Rh contents in chromitite present values up to 294 and 48 ppb, respectively (Gutierrez-Narbona et al., 2003). Minor amounts of Ru (<8 ppb) and Rh (<1.3 ppb) have been measured in fertile lherzolite (Lorand et al., 2021). Most of the PGE screened in the hyperalkaline waters were not detected with the performed analytical technique, except for Rh and, notably, Pd (2.6 to 22.7 ng/L and 28.9 to 250.1 ng/L, respectively; Table 5). Our Rh and Pd data are compatible with other studies on waters circulating in PGE rich rocks. For example, in the ultramafic Sittampundi Anorthosite Complex (India), Balaram et al. (2019) reported mean Pd and Rh concentrations in water of 744 ng/L (30–2800 ng/L) and 81 ng/L (9–339 ng/L), respectively (pH between 7.3 and 8.1). In surface waters of the Lac des Iles mine (Northwestern Ontario), Pd is 18 ng/L (Hattori and Cameron, 2004). In spring waters located in fault zones in Austria, Pd values range from 0.32 to 6.34 ng/L (Fischer et al., 2021). In geochemical exploration, in fact, Pd is a common tracer of PGE mineralization due to its greater abundance and mobility in a variety of pH values (Mountain and Wood, 1988; Hattori and Cameron, 2004; Barnes and Liu, 2012), which can explain why Pd is observed in the springs in such higher amounts instead of other PGE. In particular, Ir, Os and Ru are poorly soluble compared to Rh, Pt, and Pd (Leblanc, 1991). Therefore, our Pd data can be a proxy for PGE mineralizations in the RPM. In the RPM, PGE-rich chromitites are in fact mainly hosted within the plagioclase tectonite domain (Fig. 1; Gervilla et al., 2019 and references therein). This tectonometamorphic domain extends from N to SE of the Ronda Massif and the central sector of the Ojén Massif (Fig. 1), where chromitites outcrop. Most of the hyperalkaline springs occur either within or in contact with the chromitite-bearing plagioclase tectonite domain (AG, FA, BFA, VE, LI, BP; Fig. 1). Therefore, it is possible that these PGE-Cr-enriched chromitites may provide the catalysts required for the abiotic CH_4 synthesis via CO_2 hydrogenation, which migrates upward along faults but also is transported by hyperalkaline water.

5.4.4. Uncertainties about fluid inclusions and related high temperature FTT reactions

Fluid inclusions are sometimes invoked as a potential abiotic CH_4 source in continental serpentinization systems (Klein et al., 2019; Nothaft et al., 2021). Fluid inclusions in the RPM have not been documented in the literature. Unpublished analyses (Gervilla et al., 2019) indicate that fluid inclusions in spinel are mostly CO_2-rich. Our CH_4 clumped isotope data do not indicate high temperatures as predicted in post-magmatic fluid inclusion (>200 °C; Klein et al., 2019), and which would lead to clumped-isotope equilibrium (Young et al., 2017). The clumped-isotope disequilibrium in the CH_4 of BP and BD might be an indication of a low formation temperature, as in other cases (Young et al., 2017; Young, 2020).

6. Conclusions

The Ronda Peridotite Massifs (RPM) form the serpentinised peridotite region in Europe with the largest number (10) of verified CH_4-rich springs. Three springs show stable C and H isotope composition of CH_4 (^{13}C-depleted) typical of microbial origin and have also elevated TOC values. Five springs, of which three have been discovered in 2015 and 2021, show ^{13}C-enriched CH_4, typical of abiotic origin, and extremely

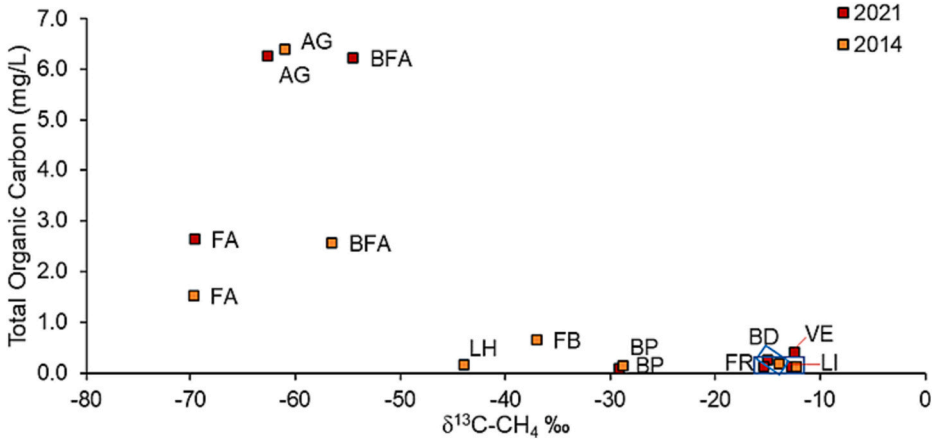

Fig. 5. Total Organic Carbon in water vs δ^{13}C of CH_4 in the RPM springs. TOC is higher for the samples with ^{13}C-depleted CH_4, typical of microbial origin. Compare symbols and δ^{13}C-CH_4 with Fig. 3. Analytical error for TOC (±0.03 mg/L) and δ^{13}C-CH_4 (± 0.1‰) are smaller than symbol size.

low TOC. CH_4 isotopes did not significantly change over a period of seven years, which reveals no substantial changes in the CH_4 source/s or post-genetic processes. The faults and shear zones where all springs occur facilitate the advective transport to the surface without altering (e.g., fractionating) the gas isotopic signature. In contrast, substantial variations were found in the contents of CH_4 and H_2, which may represent differences, over time, in migration intensity and gas pressure, and microbial activity. These temporal changes in the amount of gas released are characteristic of natural gas seepage; repeated measurements over time are necessary to better comprehend the possible quantities of gas at a specific place.

CH_4 clumped isotopes of ^{13}C-enriched gas from two sites, which are in clumped-isotope disequilibrium, are not conclusive for determining the gas origin as they lie within the overlapping microbialgenic and abiotic zones of the $^{12}CH_2D_2$ vs. $^{13}CH_3D$ diagram, (e.g., Young, 2020; Zhang et al., 2021; Etiope and Oze, 2022). However, the data are comparable to gas from other ultramafic rock systems that lack methanogens and have been interpreted as abiotic (Etiope et al., 2013; Suda et al., 2022). Consequently, the attribution of CH_4 to a microbial source based only on clumped isotopes is less conclusive than previously believed. The clumped-isotope disequilibrium is compatible with the low temperatures estimated at the base of the peridotite massif (<120 °C), which corroborates the hypothesis of CH_4 production via low temperature catalysed CO_2 hydrogenation, as opposed to high temperature synthesis in post-magmatic fluid inclusions. The presence of chromitites, contained in plagioclase tectonite layers throughout the investigated area, and of mobile and soluble PGE (Pd and Rh) in all springs, indicate availability of catalysts for CO_2 hydrogenation.

This work demonstrated once more that gas-bearing peridotite massifs, like ophiolites, are complex systems in which gas may have both abiotic and microbial origins, as well as changing emission intensities throughout time. Multiple types of data, including gas-geochemical, hydrochemical, microbiological, and mineralogical information, should be merged in a holistic manner in order to gain a comprehensive understanding of the origin and quantity of gases (CH_4 and H_2) that have the potential to be sources of energy.

Declaration of Competing Interest

The authors declare that they have no known competing financial interests or personal relationships that could have appeared to influence the work reported in this paper.

Data availability

The authors do not have permission to share data.

Acknowledgments

This article is a contribution to the Project “Hydrogeochemistry of the Ronda Peridotites: Characterization of the Groundwater and Associated Methane - UMA18-FEDERJA-101” funded by the European Regional Development Fund (FEDER) and Junta de Andalucía; and to the Project “Isotopic signatures of methane sources in the province of Málaga - B1-2022_30” funded by Universidad de Málaga. It is also a contribution to the Research Group RNM-308 (Group of Hydrogeology) and RNM-128 of the Junta de Andalucía. We thank Carina van der Veen for the stable isotope analyses of the samples. Funding charge open access: University of Malaga / CBUA.

Appendix A. Supplementary data

Supplementary data to this article can be found online at https://doi.org/10.1016/j.chemgeo.2023.121799.

References

Balaram, V., Satyanarayanan, M., Anabarasu, K., Rao, D.V.S., Dar, A.M., Kamala, C.T., Charan, S.N., 2019. Hydrogeochemistry as a tool for platinum group element (PGE) exploration-a case study from sittampundi anorthosite complex, Southern India. J. Geol. Soc. India 94 (4), 341–350. https://doi.org/10.1007/s12594-019-1321-7.

Barnes, S.J., Liu, W., 2012. Pt and Pd mobility in hydrothermal fluids: evidence from komatiites and from thermodynamic modelling. Ore Geol. Rev. 44, 49–58. https://doi.org/10.1016/j.oregeorev.2011.08.004.

Blank, J.G., Etiope, G., Stamenkovic, V., Rowe, A.R., Kohl, I., Li, S., Young, E.D., 2017. Methane at the Aqua de Ney hyperalkaline spring (N. California, USA), a site of active serpentinization. In: Astrobiol. Sci. Conf. 2017, Abstract N. 3608, April 24–28, 2017, Mesa, Arizona.

Brass, M., Röckmann, T., 2010. Continuous-flow isotope ratio mass spectrometry method for carbon and hydrogen isotope measurements on atmospheric methane. Atmos. Meas. Tech. 3, 1707–1721. https://doi.org/10.5194/amt-3-1707-2010.

Brazelton, W.J., Thornton, C.N., Hyer, A., Twing, K.I., Longino, A.A., Lang, S.Q., Lilley, M.D., Früh-Green, G.L., Schrenk, M.O., 2017. Metagenomic identification of active methanogens and methanotrophs in serpentinite springs of the Voltri Massif, Italy. PeerJ 5, e2945. https://doi.org/10.7717/peerj.2945.

Cardace, D., Meyer-Dombard, D.A.R., Woycheese, K.M., Arcilla, C.A., 2015. Feasible metabolisms in high pH springs of the Philippines. Front. Microbiol. 6, 10. https://doi.org/10.3389/fmicb.2015.00010.

Chavagnac, V., Monnin, C., Ceuleneer, G., Boulart, C., Hoareau, G., 2013. Characterization of hyperalkaline fluids produced by low-temperature serpentinization of mantle peridotites in the Oman and Ligurian ophiolites. Geochem. Geophys. Geosyst. 14 (7), 2496–2522. https://doi.org/10.1002/ggge.20147.

Costa, I.O., 2018. Deep Biosphere: Microbial Populations as Source of Biotechnological Solutions. Doctoral dissertation. Universidade de Coimbra. https://estudogeral.sib.uc.pt/handle/10316/86131.

De Melo Portella, Y., Zaccarini, F., Etiope, G., 2019. First detection of methane within chromitites of an Archean-paleoproterozoic greenstone belt in Brazil. Minerals 9 (5), 256. https://doi.org/10.3390/min9050256.

Dong, G., Xie, H., Formolo, M., Lawson, M., Sessions, A., Eiler, J., 2021. Clumped isotope effects of thermogenic methane formation: insights from pyrolysis of hydrocarbons. Geochim. Cosmochim. Acta 303, 159–183. https://doi.org/10.1016/j.gca.2021.03.009.

Eldridge, D.L., Korol, R., Lloyd, M.K., Turner, A.C., Webb, M.A., Miller III, T.F., Stolper, D.A., 2019. Comparison of experimental vs theoretical abundances of $^{13}CH_3D$ and $^{12}CH_2D_2$ for isotopically equilibrated systems from 1 to 500 C. ACS Earth Space Chem. 3 (12), 2747–2764. https://doi.org/10.1021/acsearthspacechem.9b00244.

Etiope, G., 2017. Methane origin in the Samail ophiolite. Comment on “Modern water/rock reactions in Oman hyperalkaline peridotite aquifers and implications for microbial habitability” by Miller et al. 2016. Geochim. Cosmochim. Acta 197, 467–470. https://doi.org/10.1016/j.gca.2016.08.001.

Etiope, G., 2023. Massive release of natural hydrogen from a geological seep (Chimaera, Turkey): gas advection as a proxy of subsurface gas migration and pressurised accumulations. Int. J. Hydrog. Energy 48, 9172–9184. https://doi.org/10.1016/j.ijhydene.2022.12.025.

Etiope, G., Ionescu, A., 2015. Low-temperature catalytic CO_2 hydrogenation with geological quantities of ruthenium: a possible abiotic CH_4 source in chromitite-rich serpentinized rocks. Geofluids 15 (3), 438–452. https://doi.org/10.1111/gfl.12106.

Etiope, G., Oehler, D.Z., 2019. Methane spikes, background seasonality and non-detections on Mars: a geological perspective. Planet. Space Sci. 168, 52–61. https://doi.org/10.1016/j.pss.2019.02.001.

Etiope, G., Oze, C., 2022. Microbial vs. abiotic origin of methane in continental serpentinized ultramafic rocks: a critical review and the need of a holistic approach. Appl. Geochem. 105373 https://doi.org/10.1016/j.apgeochem.2022.105373.

Etiope, G., Sherwood Lollar, B., 2013. Abiotic methane on Earth. Rev. Geophys. 51 (2), 276–299. https://doi.org/10.1016/j.marpetgeo.2013.04.009.

Etiope, G., Whiticar, M.J., 2019. Abiotic methane in continental ultramafic rock systems: Towards a genetic model. Appl. Geochem. 102, 139–152. https://doi.org/10.1016/j.apgeochem.2019.01.012.

Etiope, G., Feyzullayev, A., Baciu, C.L., 2009. Terrestrial methane seeps and mud volcanoes: a global perspective of gas origin. Mar. Pet. Geol. 26 (3), 333–344. https://doi.org/10.1016/j.marpetgeo.2008.03.001.

Etiope, G., Vance, S., Christensen, L.E., Marques, J.M., da Costa, I.R., 2013. Methane in serpentinized ultramafic rocks in mainland Portugal. Mar. Pet. Geol. 45, 12–16. https://doi.org/10.1016/j.marpetgeo.2013.04.009.

Etiope, G., Vadillo, I., Whiticar, M.J., Marques, J.M., Carreira, P.M., Tiago, I., Benavente, J., Jiménez, P., Urresti, B., 2016. Abiotic methane seepage in the Ronda peridotite massif, southern Spain. Appl. Geochem. 66, 101–113. https://doi.org/10.1016/j.apgeochem.2015.12.001.

Etiope, G., Ifandi, E., Nazzari, M., Procesi, M., Tsikouras, B., Ventura, G., Steele, A., Tardini, R., Szatmari, P., 2018. Widespread abiotic methane in chromitites. Sci. Rep. 8 (1), 1–10. https://doi.org/10.1038/s41598-018-27082-0.

Fernàndez, M., Marzán, I., Correia, A., Ramalho, E., 1998. Heat flow, heat production, and lithospheric thermal regime in the Iberian Peninsula. Tectonophysics 291 (1–4), 29–53. https://doi.org/10.1016/S0040-1951(98)00029-8.

Fischer, L., Moser, B., Hann, S., 2021. Determination of background concentrations of Ag, Pd, Pt and Au in highly mineralized ground waters at Sub-ng L–1 concentrations by online matrix separation/pre-concentration coupled to ICP-SFMS. Molecules 26 (23), 7253. https://doi.org/10.3390/molecules26237253.

Fones, E.M., Templeton, A.S., Mogk, D.W., Boyd, E.S., 2022. Transformation of low-molecular-weight organic acids by microbial endoliths in subsurface mafic and ultramafic igneous rock. Environ. Microbiol. 24 (9), 4137–4152. https://doi.org/10.1111/1462-2920.16041.

García-Dueñas, V., Balanyá, J.C., Martínez-Martínez, J.M., 1992. Miocene extensional detachments in the outcropping basement of the northern Alboran basin (Betics) and their tectonic implications. Geo-Mar. Lett. 12 (2), 88–95. https://doi.org/10.1007/BF02084917.

Gervilla, F., González Jiménez, J.M., Hidas, K., Marchesi, C., Piña, R., 2019. Geology and Metallogeny of the Upper Mantle Rocks from the Serranía de Ronda. http://hdl.handle.net/10261/206926.

Giampouras, M., Garrido, C.J., Zwicker, J., Vadillo, I., Smrzka, D., Bach, W., Peckmann, J., Jiménez, P., Benavente, J., García-Ruiz, J.M., 2019. Geochemistry and mineralogy of serpentinization-driven hyperalkaline springs in the Ronda peridotites. Lithos 350, 105215. https://doi.org/10.1016/j.lithos.2019.105215.

Gooddy, D.C., Hinsby, K., 2008. Organic quality of groundwaters. In: Natural Groundwater Quality, pp. 59–70. https://doi.org/10.1002/9781444300345.ch3.

Grozeva, N.G., Klein, F., Seewald, J.S., Sylva, S.P., 2020. Chemical and isotopic analyses of hydrocarbon-bearing fluid inclusions in olivine-rich rocks. Phil. Trans. R. Soc. A 378, 20180431. https://doi.org/10.1098/rsta.2018.0431.

Gutierrez-Narbona, R., Lorand, J.P., Gervilla, F., Gros, M., 2003. New data on base metal mineralogy and platinum-group minerals in the Ojen chromitites (Serrania de Ronda, Betic Cordillera, southern Spain). N. Jb. Mineral. (Abh.) 179 (2), 143–173. https://doi.org/10.1127/0077-7757/2003/0179-0143.

Hattori, K.H., Cameron, E.M., 2004. Using the high mobility of palladium in surface media in exploration for platinum group element deposits: evidence from the Lac des Iles region, northwestern Ontario. Econ. Geol. 99 (1), 157–171. https://doi.org/10.2113/gsecongeo.99.1.157.

Hernández- Pacheco, A., 1967. Estudio petrográfico y geoquímico del macizo ultramáfico de Ojén (Málaga). Estud. Geol. XXIII 85–143.

Hidas, K., Booth-Rea, G., Garrido, C.J., Martínez-Martínez, J.M., Padrón-Navarta, J.A., Konc, Z., Giaconia, F., Frets, E., Marchesi, C., 2013. Backarc basin inversion and subcontinental mantle emplacement in the crust: kilometre-scale folding and shearing at the base of the proto-Alborán lithospheric mantle (Betic Cordillera, southern Spain). J. Geol. Soc. Lond. 170 (1), 47–55. https://doi.org/10.1144/jgs2011-151.

Hinrichs, K.U., Hayes, J.M., Bach, W., Spivack, A.J., Hmelo, L.R., Holm, N.G., Johnson, C.G., Sylva, S.P., 2006. Biological formation of ethane and propane in the deep marine subsurface. Proc. Natl. Acad. Sci. Unit. States Am. 103, 14684–14689. https://doi.org/10.1073/pnas.060653510.

Jiménez-Gavilán, P.J., Vadillo, I., Gallardo, R.S., 2021. Caracterización hidrogeoquímica e isotópica preliminar de los manantiales epiperidotíticos de las Peridotitas de Ronda. Geotemas 18, 303–307. https://sge.usal.es/archivos/GEO_TEMAS/Geo_temas18.pdf.

Klein, F., Grozeva, N.G., Seewald, J.S., 2019. Abiotic methane synthesis and serpentinization in olivine-hosted fluid inclusions. Proc. Natl. Acad. Sci. U. S. A. 116 (36), 17666–17672. https://doi.org/10.1073/pnas.1907871116.

Labidi, J., Young, E.D., Giunta, T., Kohl, I.E., Seewald, J., Tang, H., Lilley, M.D., Früh-Green, G.L., 2020. Methane thermometry in deep-sea hydrothermal systems: evidence for re-ordering of doubly-substituted isotopologues during fluid cooling. Geochim. Cosmochim. Acta 288, 248–261. https://doi.org/10.1016/j.gca.2020.08.013.

Leblanc, M., 1991. Platinum-group elements and gold in ophiolitic complexes: distribution and fractionation from Mantle to Oceanic floor. In: Peters, T., Nicolas, A., Coleman, R.G. (Eds.), Ophiolite Genesis and Evolution of the Oceanic Lithosphere. Petrology and Structural Geology, vol 5. Springer, Dordrecht. https://doi.org/10.1007/978-94-011-3358-6_13.

Lorand, J., Pont, S., Guttierez-Narbona, R., Gervilla, F., 2021. Chalcophile-siderophile element systematics and regional-scale magmatic percolation in the Ronda peridotite massif (Spain). Lithos 380-381, 105901. https://doi.org/10.1016/j.lithos.2020.105901.

McDermott, J.M., Seewald, J.S., German, C.R., Sylva, S.P., 2015. Pathways for abiotic organic synthesis at submarine hydrothermal fields. Proc. Natl. Acad. Sci. U. S. A. 112 (25), 7668–7672. https://doi.org/10.1073/pnas.1506295112.

Milkov, A.V., Etiope, G., 2018. Revised genetic diagrams for natural gases based on a global dataset of > 20,000 samples. Org. Geochem. 125, 109–120. https://doi.org/10.1016/j.orggeochem.2018.09.002.

Miller, H.M., Matter, J.M., Kelemen, P., Ellison, E.T., Conrad, M.E., Fierer, N., Ruchala, T., Tominaga, M., Templeton, A.S., 2016. Modern water/rock reactions in Oman hyperalkaline peridotite aquifers and implications for microbial habitability. Geochim. Cosmochim. Acta 179, 217–241. https://doi.org/10.1016/j.gca.2016.01.033.

Miller, H.M., Chaudhry, N., Conrad, M.E., Bill, M., Kopf, S.H., Templeton, A.S., 2018. Large carbon isotope variability during methanogenesis under alkaline conditions. Geochim. Cosmochim. Acta 237, 18–31. https://doi.org/10.1016/j.gca.2018.06.007.

Monnin, C., Quéméneur, M., Price, R., Jeanpert, J., Maurizot, P., Boulart, C., Donval, J. P., Pelletier, B., 2021. The chemistry of hyperalkaline springs in serpentinizing environments: 1. The composition of free gases in New Caledonia compared to other springs worldwide. Eur. J. Vasc. Endovasc. Surg. 126 (9), e2021JG006243 https://doi.org/10.1029/2021JG006243.

Morrill, P.L., Kuenen, J.G., Johnson, O.J., Suzuki, S., Rietze, A., Sessions, A.L., Fogel, M. L., Nealson, K.H., 2013. Geochemistry and geobiology of a present-day serpentinization site in California: the Cedars. Geochim. Cosmochim. Acta 109, 222–240. https://doi.org/10.1016/j.gca.2013.01.043.

Mountain, B.W., Wood, S.A., 1988. Solubility and transport of platinum-group elements in hydrothermal solutions: thermodynamic and physical chemical constraints. In: Prichard, H.M., Potts, P.J., Bowles, J.F.W., Cribb, S.J. (Eds.), Geo-Platinum, 87. Springer, Dordrecht. https://doi.org/10.1007/978-94-009-1353-0_8.

Nothaft, D.B., Templeton, A.S., Rhim, J.H., Wang, D.T., Labidi, J., Miller, H.M., Boyd, E. S., Matter, J.M., Ono, S., Young, E.D., Kopf, S.H., Kelemen, P.B., Conrad, M.E., Oman Drilling Project Science Team, 2021. Geochemical, biological, and clumped isotopologue evidence for substantial microbial methane production under carbon limitation in serpentinites of the Samail Ophiolite, Oman. J. Geophys. Res. Biogeosci. 126 (10), e2020JG006025 https://doi.org/10.1029/2020JG006025.

Obata, M., 1980. The Ronda peridotite-garnet-lherzolite, spinel-lherzolite, and plagioclase-lherzolite facies and the PT trajectories of a high-temperature mantle Intrusion. J. Petrol. 21 (3), 533–572. https://doi.org/10.1093/petrology/21.3.533.

Oremland, R.S., Whiticar, M.J., Strohmaier, F.E., Kiene, R.P., 1988. Bacterial ethane formation from reduced, ethylated sulfur compounds in anoxic sediments. Geochim. Cosmochim. Acta 52, 1895–1904. https://doi.org/10.1016/0016-7037(88)90013-0.

Platt, J.P., Behr, W.M., Johanesen, K., Williams, J.R., 2013. The Betic-Rif arc and its orogenic hinterland: a review. Annu. Rev. Earth Planet. Sci. 41, 313–357. https://doi.org/10.1146/annurev-earth-050212-123951.

Sherwood Lollar, B., Lacrampe-Couloume, G., Slater, G.F., Ward, J., Moser, D.P., Gihring, T.M., Lin, L.H., Onstott, T.C., 2006. Unravelling abiogenic and biogenic sources of methane in the Earth's deep subsurface. Chem. Geol. 226 (3–4), 328–339. https://doi.org/10.1016/j.chemgeo.2005.09.027.

Röckmann, T., Eyer, S., van der Veen, C., Popa, M.E., Tuzson, B., Monteil, G., Houweling, S., Harris, E., Brunner, D., Fischer, H., Zazzeri, G., Lowry, D., Nisbet, E. G., Brand, W.A., Necki, J.M., Emmenegger, L., Mohn, J., 2016b. In situ observations of the isotopic composition of methane at the Cabauw tall tower site. Atmos. Chem. Phys. 16, 10469–10487. https://doi.org/10.5194/acp-16-10469-2016.

Röckmann, T., Popa, M.E., Krol, M.C., Hofmann, M.E.G., 2016a. Statistical clumped isotope signatures. Sci. Rep. 6, 31947. https://doi.org/10.1038/srep31947.

Sherwood Lollar, B., Heuer, V., McDermott, J., Tille, S., Warr, O., Moran, J., Telling, J., Hinrichs, K., 2021. A window into the abiotic carbon cycle – Acetate and formate in fracture waters in 2.7 billion year-old host rocks of the Canadian Shield. Geochim. Cosmochim. Acta 294, 295–314. https://doi.org/10.1016/j.gca.2020.11.026.

Sivan, M., Röckmann, T., van der Veen, C., Popa, M.E., 2023. Extraction, purification, and clumped isotope analysis of methane ($\Delta_{13}CDH_3$ and $\Delta^{12}CD_2H_2$) from sources and the atmosphere. EGUsphere 1-35. https://doi.org/10.5194/egusphere-2023-1906.

Stolper, D.A., Lawson, M., Formolo, M.J., Davis, C.L., Douglas, P.M., Eiler, J.M., 2018. The utility of methane clumped isotopes to constrain the origins of methane in natural gas accumulations. Geol. Soc. Spec. Publ. 468 (1), 23–52. https://doi.org/10.1144/SP468.3.

Suda, K., Ueno, Y., Yoshizaki, M., Nakamura, H., Kurokawa, K., Nishiyama, E., Yoshino, K., Hongoh, Y., Kawachi, K., Omori, S., Yamada, K., Yoshida, N., Maruyama, S., 2014. Origin of methane in serpentinite-hosted hydrothermal systems: the CH_4–H_2–H_2O hydrogen isotope systematics of the Hakuba Happo hot spring. Earth Planet. Sci. Lett. 386, 112–125. https://doi.org/10.1016/j.epsl.2013.11.001.

Suda, K., Aze, T., Miyairi, Y., Yokoyama, Y., Matsui, Y., Ueda, H., Saito, T., Sato, T., Sawaki, Y., Nakai, R., Tamaki, H., Takahashi, H.A., Morikawa, N., Ono, S., 2022. The origin of methane in serpentinite-hosted hyperalkaline hot spring at Hakuba Happo, Japan: radiocarbon, methane isotopologue and noble gas isotope approaches. Earth Planet. Sci. Lett. 585, 117510 https://doi.org/10.1016/j.epsl.2022.117510.

Szponar, N., Brazelton, W.J., Schrenk, M.O., Bower, D.M., Steele, A., Morrill, P.L., 2013. Geochemistry of a continental site of serpentinization, the Tablelands Ophiolite, Gros Morne National Park: a mars analogue. Icarus 224 (2), 286–296. https://doi.org/10.1016/j.icarus.2012.07.004.

Taenzer, L., Labidi, J., Masterson, A.L., Feng, X., Rumble III, D., Young, E.D., Leavitt, W. D., 2020. Low $\Delta^{12}CH_2D_2$ values in microbialgenic methane result from combinatorial isotope effects. Geochim. Cosmochim. Acta 285, 225–236. https://doi.org/10.1016/j.gca.2020.06.026.

Tiago, I., Veríssimo, A., 2013. Microbial and functional diversity of a subterrestrial high pH groundwater associated to serpentinization. Environ. Microbiol. 15 (6), 1687–1706. https://doi.org/10.1111/1462-2920.12034.

Umezawa, T., Brenninkmeijer, C.A.M., Röckmann, T., van der Veen, C., Tyler, S.C., Fujita, R., Morimoto, S., Aoki, S., Sowers, T., Schmitt, J., Bock, M., Beck, J., Fischer, H., Michel, S.E., Vaughn, B.H., Miller, J.B., White, J.W.C., Brailsford, G., Schaefer, H., Sperlich, P., Brand, W.A., Rothe, M., Blunier, T., Lowry, D., Fisher, R.E., Nisbet, E.G., Rice, A.L., Bergamaschi, P., Veidt, C., Levin, I., 2018. Interlaboratory comparison of $\delta^{13}C$ and δD measurements of atmospheric CH_4 for combined use of data sets from different laboratories. Atmos. Meas. Tech. 11 (2), 1207–1231. https://doi.org/10.5194/amt-11-1207-2018.

Vadillo, I., Urresti, B., Jiménez, P., Martos, S., José Durán, J., Benavente, J., Carrasco, F., Pedrera, A., 2016. Preliminary hydrochemical study of Ronda ultramafic massif (South Spain). In: EGU General Assembly Conference Abstracts, EPSC2016-13275.

Wang, D.T., Welander, P.V., Ono, S., 2016. Fractionation of the methane isotopologues $^{13}CH_4$, $^{12}CH_3D$, and $^{13}CH_3D$ during aerobic oxidation of methane by *Methylococcus capsulatus* (Bath). Geochem. Cosmochim. Acta 192, 186–202. https://doi.org/10.1016/j.gca.2016.07.031.

Warr, O., Young, E.D., Giunta, T., Kohl, I.E., Ash, J.L., Lollar, B.S., 2021. High-resolution, long-term isotopic and isotopologue variation identifies the sources and sinks of methane in a deep subsurface carbon cycle. Geochem. Cosmochim. Acta 294, 315–334. https://doi.org/10.1016/j.gca.2020.12.002.

Woycheese, K.M., Meyer-Dombard, D.A.R., Cardace, D., Argayosa, A.M., Arcilla, C.A., 2015. Out of the dark: transitional subsurface-to-surface microbial diversity in a terrestrial serpentinizing seep (Manleluag, Pangasinan, the Philippines). Front. Microbiol. 6, 44. https://doi.org/10.3389/fmicb.2015.00044.

Wyatt, D.E., Richers, D.M., Pirkle, R.J., 1995. Barometric pumping effects on soil gas studies for geological and environmental characterization. Environ. Geol. 25 (4), 243–250. https://doi.org/10.1007/BF00766753.

Xie, S., Lazar, C.S., Lin, Y., Teske, A., Hinrichs, K., 2013. Ethane- and propane-producing potential and molecular characterization of an ethanogenic enrichment in an anoxic estuarine sediment. Org. Geochem. 59, 37–48. https://doi.org/10.1016/j.orggeochem.2013.03.001.

Young, E.D., 2020. A two-dimensional perspective on CH_4 isotope clumping: distinguishing process from source. In: Orcutt, B.N., Daniel, I., Dasgupta, R. (Eds.), Deep Carbon: Past to Present, 1029, pp. 388–414.

Young, E.D., Kohl, I.E., Lollar, B.S., Etiope, G., Rumble III, D., Li, S., Haghnegahdar, M.A., Schauble, E.A., McCain, K.A., Foustoukos, D.I., Sutclife, C., Warr, O., Ballentine, C.J., Onstott, T.C., Hosgormez, H., Neubeck, A., Marques, J.M., Pérez-Rodríguez, I., Rowe, A.R., LaRowe, D.E., Magnabosco, C., Yeung, L.Y., Ash, J.L., Bryndzia, L.T., 2017. The relative abundances of resolved $^{12}CH_2D_2$ and $^{13}CH_3D$ and mechanisms controlling isotopic bond ordering in abiotic and biotic methane gases. Geochim. Cosmochim. Acta 203, 235–264. https://doi.org/10.1016/j.gca.2016.12.041.

Zhang, N., Sekine, Y., Yamada, K., Nakagawa, M., Lin, M., Yoshida, N., 2021. Clumped isotope signatures of abiotic methane formed via nickel-catalyzed Fischer-Tropsch synthesis and their implications. In: AGU Fall Meeting Abstracts 2021, P25B-2170.

Zwicker, J., Smrzka, D., Vadillo, I., Jiménez-Gavilán, P., Giampouras, M., Peckmann, J., Bach, W., 2022. Trace and rare earth element distribution in hyperalkaline serpentinite-hosted spring waters and associated authigenic carbonates from the Ronda peridotite. Appl. Geochem. 147, 105492 https://doi.org/10.1016/j.apgeochem.2022.105492.